Manuscript submitted to
AIMS' Journals
Volume **X**, Number **0X**, XX **200X**

doi:10.3934/xx.xx.xx.xx

pp. **X–XX**

A COMPARISON OF SOME NUMERICAL CONFORMAL MAPPING METHODS FOR SIMPLY AND MULTIPLY CONNECTED DOMAINS

M. Badreddine, T. K. DeLillo*, and S. Sahraei

Department of Mathematics, Statistics, and Physics
Wichita State University
Wichita, KS 67260-0033, USA

(Communicated by the associate editor name)

Abstract. This paper compares some methods for computing conformal maps from simply and multiply connected domains bounded by circles to target domains bounded by smooth curves and curves with corners. We discuss the use of explicit preliminary maps, including the osculation method of Grassmann, to first conformally map the target domain to a more nearly circular domain. The Fourier series method due to Fornberg and its generalization to multiply connected domains are then applied to compute the maps to the nearly circular domains. The final map is represented as a composition of the Fourier/Laurent series with the inverted explicit preliminary maps. A method for systematically removing corners with power maps is also implemented and composed with the Fornberg maps. The use of explict maps has been suggested often in the past, but has rarely been carefully studied, especially for the multiply connected case. Using Fourier series to represent conformal maps from domains bounded by circles to more general domains has certain computational advantages, such as the use of fast methods. However, if the target domain has elongated sections or corners, the mapping problems can suffer from severe ill-conditioning or loss of accuracy. The purpose of this paper is to illustrate some of these practical possibilites and limitations.

1. **Introduction.** This paper compares some methods for computing conformal maps from simply and multiply connected domains bounded by circles to target domains bounded by smooth curves and curves with corners. We discuss the use of explicit preliminary maps, including the osculation method of Grassmann [17], to conformally map the target domain to a more nearly circular domain. The Fourier series method due to Fornberg [15] and its generalization to multiply connected domains [3] are then applied to compute the maps to the nearly circular domains. The final map is represented as a composition of the Fourier/Laurent series with the inverted explicit preliminary maps. A novel method for systematically removing corners with power maps is also implemented and composed with the Fornberg maps (which require smooth boundaries) and the level of error that can be expected when using Fourier series to treat domains with corners is illustrated by comparing the results with the Schwarz-Christoffel mapping from SC Toolbox [14] .

We also report some preliminary attempts to combine the Fornberg-like method with Karman-Trefftz method for removing trailing edge corners in multi-element airfoils. This is a classic method for computing potential flow over airfoils; see, e.g., [9, 21, 45].

Preliminary explicit maps which map a given domain to a more nearly circular domain or smooth corners have been used frequently [18, 21, 25, 29, 32, 40]. However, systematic comparisons

2010 *Mathematics Subject Classification.* Primary: 30C30, 65E05.

Key words and phrases. Numerical conformal mapping, multiply connected domains, Fornberg's method, Grassmann's method, osculation methods, potential flow.

* Corresponding author: T. K. DeLillo.

of various approaches are difficult to find. Here we revisit some of the calculations from [4] (see also [5, 6]) and extend them to multiply connected domains and domains with corners. Parts of this work appeared in the first author's PhD dissertation [2] where sections of our MATLAB code are included to show specific examples of the implementations. General introductions to numerical conformal mapping and collections of maps are given in [16, 22, 24, 28, 39]. Wegmann [44] gives an overview and many computational examples and references.

Most applications of conformal mapping involve transplanting boundary value problems for the Laplace equation to a domain, such as the unit disk, where the problem can be solved efficiently. For domains far from the disk, such as an elongated or pinched domain, the map can have large distortions making the numerical problem highly ill-conditioned and requiring many mesh points to achieve sufficient accuracy. We give examples of such domains below in order to illustrate the limits of usefulness of the methods. However, for moderate geometries with sufficiently smooth boundaries and data, these series-based methods lead to fast, spectrally accurate methods.

This paper is organized as follows. Section 2 treats simply connected domains. After recalling the Riemann Mapping Theorem, a short exposition of our modification of Fornberg's original method [15] for the simply connected case is given along with a brief review of a method for fitting points on the boundaries with a periodic cubic spline parametrized by chordal arc length. This is necessary, since the explicit maps transform a (finite) distribution of points along the boundaries and Fornberg's method requires the final boundary to be defined as a smooth, parametrized curve. Grassmann's method [17] for mapping the original boundary to a more circular boundary using a composition $g = g_{igm} \circ \cdots g_2 \circ g_1$ of explicit preliminary maps g_i is explained. Numerical examples are then discussed illustrating our calculations for simply connected domains. We then compute the Fornberg map h from the unit disk to the near circle domain and compose it with the inverted Grassmann map g^{-1} , so that the final map is $f = g^{-1} \circ h$; see Figure 1 for an example. This approach is compared with the direct calculation of f from the disk to the original domain by Fornberg's method. The errors were calculated and graphed for several values of $N = 2^M$ Fourier points for some popular families of test cases, including inverted ellipses, where the explicit maps are known and problems can be made more difficult by making the domains "thinner". The rest of the section discusses a method for smoothing corners by power maps using a new Koebe-like method. In Example 5, we remove the corners of the square, apply Fornberg's method to the resulting domain, and finally invert the Koebe-like maps. In Table 4, the results are compared to the Schwarz-Christoffel map from SC Toolbox [14], which gives essentially exact results for polygonal domains.

Section 3 discusses the extension of Fornberg's method to the exterior multiply connected case of connectivity $m \geq 2$ developed in [3]. The first numerical example uses the region containing the point at infinity and bounded by three inverted ellipses and one ellipse. We apply Grassmann mappings to each inverted ellipse and the ellipse successively to conformally map the target domain to a more nearly circular domain. The process is a composition of Fornberg maps and inverted Grassmann maps g similar to the simply connected cases in Section 2. The second part covers a method for removing corners in exterior multiply connected domains. The Koebe-like method from Section 2 is used to remove multiple corners from each boundary curve of three rectangles after first inverting in a circle; see Figure 24, below.

In Section 4, we discuss the classical Karman-Trefftz transformation k for removing single trailing-edge corners from an airfoil domain and calculating potential flow. The final map is then $k^{-1} \circ h$, where h is the Fornberg map to the smooth domain. Flow over a single-element and a two-element airfoil are shown, similar to the setup in [21].

Section 5 briefly discusses the bounded, multiply connected case and Section 6 states some conclusions and directions for future research.

2. **Simply connected domains.** We recall the Riemann mapping theorem for a simply connected domain.

Theorem 2.1. *Let Ω be a simply connected region which is not the whole plane or the Riemann sphere, and let a be a point of Ω. Then there exists in Ω a unique analytic function g satisfying the conditions*

$$g(a) = 0 \quad \text{and} \quad g'(a) > 0,$$

and assuming every value in the unit disk $D = \{w : |w| < 1\}$ exactly once.

Recall that for conformal maps, $g'(z) \neq 0$, so that the directions of the curves passing through any point are unchanged. For the proof of the mapping theorem, see, e.g., [1, pp. 325–326]. We

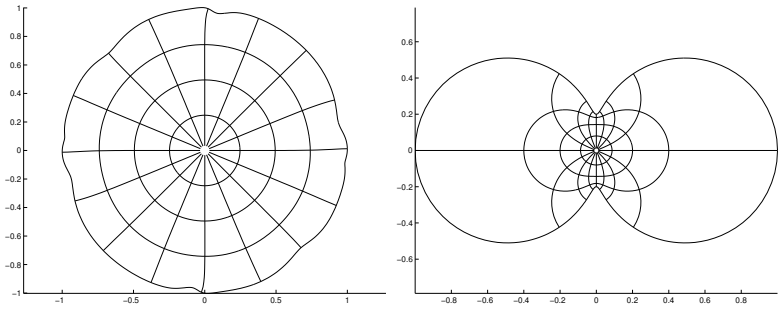

FIGURE 1. The composition $f = g^{-1} \circ h$ of Fornberg map h using $N = 256$ Fourier points from unit disk to the near circle $g(\Gamma)$ (left), where Γ is the inverted ellipse with $\alpha = 0.2$ (right), produced with composition of 10 Grassmann maps $g = g_{10} \circ \cdots g_2 \circ g_1$.

will mainly be interested in numerically approximating the inverse of the Riemann map, $f = g^{-1}$. (In fact, the composition of the explicit maps can be viewed as an approximation to g.)

2.1. **Fornberg's method for the disk.** Fornberg [15] proposed a method for computing the conformal map f from the interior of the unit disk to the interior of a smooth, closed curve. We use a slight modification of Fornberg's original formulation which we review briefly here; see [8, 13, 43, 44] for details.

We want to find the conformal map from the interior of unit disk D onto the interior Ω of a Jordan curve Γ. Consider the boundary Γ of Ω to be parametrized by S (e.g., arclength or polar angle), $\Gamma : \gamma(S), 0 \le S \le L, \gamma(0) = \gamma(L)$. The normalization imposed on f is $f(0) = a \in \Omega$ and $f(1) = \gamma(0)$. Finding f is equivalent of finding the boundary correspondence, $S = S(\theta)$ such that $f(e^{i\theta}) = \gamma(S(\theta))$. If f has the expansion

$$f(e^{i\theta}) = \sum_{k=-\infty}^{\infty} a_k e^{ik\theta},$$

then f extends analytically into D if and only if

$$a_{-k} = \frac{1}{2\pi} \int_0^{2\pi} f(e^{i\theta}) e^{ik\theta} dt = 0, \ k = 1, 2, \ldots;$$

see [24, Sec. 14.3.1].

A Newton-like method is used for numerically solving for the boundary correspondence function $S(\theta)$. Let $S^k(\theta)$ be an approximation to the boundary correspondence function $S(\theta)$ at the kth Newton step. We need to find a 2π-periodic correction $U^k(\theta)$ such that $f(e^{i\theta}) = \gamma(S^k(\theta) + U^k(\theta))$ are the boundary values at $e^{i\theta}$ of the conformal mapping f. Since it is difficult to find the desired correction $U^k(\theta)$, we compute the correction by linearizing about $S^k(\theta)$,

$$f(e^{i\theta}) \approx \gamma(S^k(\theta)) + \gamma'(S^k(\theta)) U^k(\theta).$$

The condition that the values should have negatively indexed Taylor coefficients leads to a linear problem for the unknown U^k. The system is discretized with N-point trigonometric interpolation and results in a symmetric positive definite system,

$$A\underline{U} = \underline{b},$$

where A is the discretization the identity plus a low rank operator. The system can be solved efficiently with the conjugate gradient method with matrix-vector multiplication using the `fft` at a cost of $O(N \log N)$. The Newton update is then

$$S^{k+1}(\theta) = S^k(\theta) + U^k(\theta)$$

and near-quadratic convergence is generally observed for a sufficiently close initial guess; see Tables 1 and 5. Usually $S^0(\theta) = L\theta/2\pi$ will work for domains that aren't too far from circular.

Once the boundary correspondence is found, we can easily find the Taylor series, $f(z) = \sum_{k=0}^{\infty} a_k z^k$, for the map. For $|z| < |\zeta| = 1, \zeta = e^{i\theta}, d\zeta = ie^{i\theta} d\theta$

$$\begin{aligned} f(z) &= \frac{1}{2\pi i} \int_{|\zeta|=1} \frac{\gamma(S(\theta))}{\zeta - z} d\zeta \\ &= \frac{1}{2\pi i} \int_{|\zeta|=1} \gamma(S(\theta)) \left(1 + \frac{z}{\zeta} + \left(\frac{z}{\zeta}\right)^2 + \cdots\right) \frac{d\zeta}{\zeta} \\ &= \sum_{k=0}^{\infty} \left(\frac{1}{2\pi} \int_0^{2\pi} \gamma(S(\theta)) e^{-ik\theta} d\theta\right) z^k = \sum_{k=0}^{\infty} a_k z^k. \end{aligned}$$

Therefore the Taylor coefficients of $f(z)$ are the Fourier coefficients of the 2π-periodic function, $\gamma(S(\theta))$, $a_k := \frac{1}{2\pi} \int_0^{2\pi} \gamma(S(\theta)) e^{-ik\theta} d\theta$.

2.2. **Parametrizing the boundary.** Piecewise smooth boundaries may be given by analytic formulas. However, the preliminary maps are constructed by successively conformally transforming a finite set of boundary points. The resulting curve must be parametrized in order to apply Fornberg's method. We fit the points by two periodic cubic splines—one for the x coordinates and one for the y coordinates—parametrized by the chordal arclength between two successive points $(x_k, y_k), k = 1, \ldots, Ns$ along the boundary. Our MATLAB code is based on [26]. A smoother fit to the boundary points may be computed with trigonometric interpolation. However, as we show in an example below, this does not to result in much improvement in our computations.

2.3. **Numerical examples using Fornberg's method for analytic boundaries.** In this section, we apply the Fornberg map directly and in combination with preliminary Grassmann maps to some explicity known test cases. The calculated errors for the direct Fornberg (Taylor series) map for analytic parametrization of the boundary exhibit spectral accuracy, that is, doubling the number of Fourier points N (or equivalently, the number of Taylor coefficients $N/2$), squares the error, as expected, since the Taylor coefficients decay geometrically. We consider two examples of test cases for families of curves: the family of inverted ellipses and the family of ellipses; see [7] for other test cases. Each family has a parameter, such as the "thinness" $0 < \alpha \leq 1$ of the domain, that can be changed to make a more poorly conditioned problem requiring larger N to maintain accuracy as $\alpha \to 0$; see [7] for details. Fornberg's method may not converge using the standard initial guess, whereas, Fornberg maps to near circles produced by preliminary Grassmann maps don't require special initial guesses. One could use the preliminary map procedure to generate a good initial guess to Fornberg's direct method for difficult domains, but we have not tried this.

Example 1 (Inverted Ellipse)**.** The boundary curve for the inverted ellipse is

$$\Gamma : \gamma(S) = \rho(S) e^{iS}, \quad 0 \leq S \leq 2\pi, \quad \text{where} \quad \rho(S) = \sqrt{1 - (1 - \alpha^2) \sin^2 S}.$$

$0 < \alpha < 1$ is the distance of 0 to the nearest boundary point. The exact map is

$$w = f(z) = \frac{2\alpha z}{1 + \alpha - (1 - \alpha) z^2}.$$

Note: This map can be derived from the Joukowski map $f(z) = z + 1/z$ which maps exteriors of circles to exteriors of ellipses by inverting, normalizing properly, and rotating. The images of a polar coordinate grid in the interior of the disk under the conformal mapping is displayed in Figure 2. In this case Fornberg's method usually converges with 10 Newton iterations or fewer when the initial guess for the boundary correspondence is given as the standard initial guess, $S^0(\theta) := L\theta/2\pi$, where here $L = 2\pi$. Quadratic convergence for this analytic boundary parametrization is shown in Table 1. The convergence rate is generally somewhat slower for spline boundaries; see Table 5. The errors in Figure 3 for an analytic parametrization of the boundary exhibit spectral accuracy and are better than the results using preliminary Grassmann maps, Figure 11. However, for $\alpha = 0.1$ and $N = 64, 128$, Fornberg's method did not converge using the standard initial guess, whereas, Fornberg maps to near circles produced by preliminary Grassmann maps don't require special initial guesses.

In practice, a boundary curve might be represented by a finite set of points fitted with a periodic cubic spline and spectral accuracy will not be a possibility. Boundary points can be fitted using trigonometric interpolation in an effort to achieve higher accuracy; see, e.g., [37, Fig. 13]. Table 2 gives errors and timings for inverted ellipses, with 10 preliminary Grassmann maps, comparing accuracy and timings for trigonometric interpolation and cubic spline interpolation of the Ns nearly

circular mapped points. There is only a slight gain in accuracy in some cases using trigonometric interpolation. The points interpolated are not equidistant. Also, the interpolant must be evaluated at the N Fourier points at each Newton iteration of the Fornberg map to the near-circles. For the cubic spline interpolant, this costs $O(N)$ flops. Since the conjugate gradient iterations for the inner linear systems for Fornberg's method generally converges superlinearly, Fornberg's method costs $O(N \log N)$ using splines (or analytic formulas) for $\gamma(S)$. (In general, computing the direct map to the domain is slightly faster than using preliminary Grassmann maps with spline interpolation.) However, it costs $O(N \cdot Ns)$ flops per Newton step to evaluate the Ns-point trigonometric interpolant at the N Fourier points, since the fft cannot be used for the non-equidistant points and it would cost more than $O(N)$, in any case. The timings in Table 2 for trigonometric interpolation are nearly 10 times greater than for spline interpolation. The small advantage of generating a smoother interpolant with trigonometric interpolation of the very unevenly distributed mapped points thus seems to be lost. It is also necessary to do an additional spline fit to generate a good initial guess of equally distributed points for the Fornberg map to the near circle, since equally distributed points in the trigonometric parameter are not equally distributed on the near circle. If this is not done, the Fornberg iteration will usually not converge. If higher accuracy is needed using the Grassmann maps, it can be achieved by taking large values of Ns (and N) as shown in Figure 12.

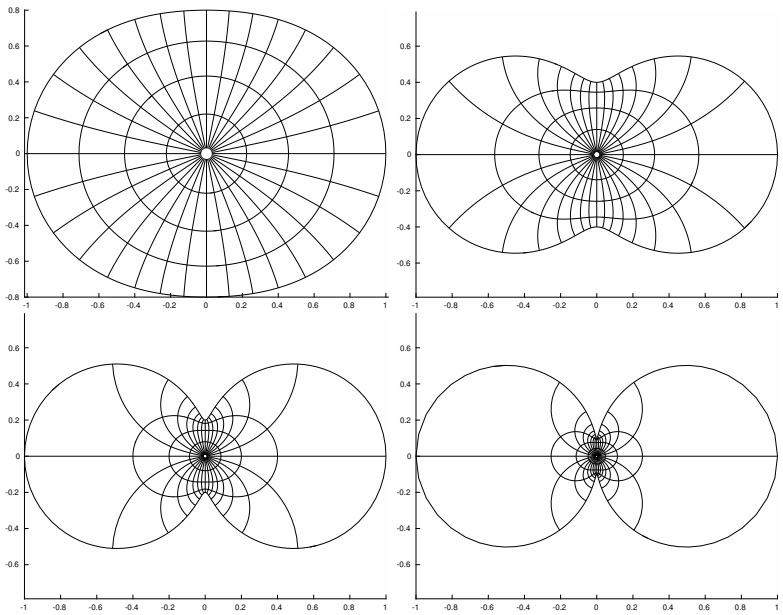

FIGURE 2. Fornberg maps to inverted ellipses with $\alpha = 0.8, 0.4, 0.2, 0.1$ and $N = 64, 128, 256, 256$, resp..

Example 2 (Ellipse)**.** See Figure 4. This is an example of an elongated region analyzed in [7]. Maps from the disk to an elongated region have distortions that increase exponentially with the aspect ratio of the region causing very severe ill-condtioning and limiting the applicability of Fourier series methods. It was originally hoped that the use of preliminary maps might circumvent this ill-conditioning, but the large distortions are transferred to the preliminary maps which then amplify any errors in the Fourier series map to the near circle. Two crescent maps are generally enough to map ellipse domains to very-nearly circular domains.

For our calculations, we use the analytic, starlike parametrization of the boundary of the ellipse, $\gamma(S) = \rho(S)e^{iS}$, where $\rho(S) = \alpha/\sqrt{1-(1-\alpha^2)\cos^2(S)}$ and $0 < \alpha \leq 1$. However, for thin ellipses, using the parametrization $\gamma(S) = \cos(S) + i\alpha\sin(S)$ or using a spline fit with, say $Ns = 2000$ knots makes little difference. Note that the conformal map satisfies $f(0) = 0, f(\pm 1) = \pm 1$, and

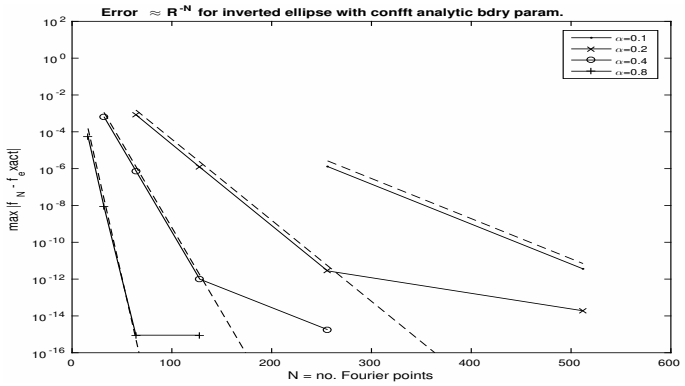

FIGURE 3. Errors for Fornberg maps to inverted ellipse with analytic boundary.

TABLE 1. Convergence of successive iteration errors at the Fourier points for the map to an inverted ellipse with $\alpha = 0.2$ and $N = 128$. Note that the discrete problem is solved to machine precision but the truncation error is limited by N.

Iteration	$\|S^{k+1} - S^k\|_\infty$	$\|f_{computed} - f_{exact}\|_\infty$
1	6.0e-01	6.6e-01
2	3.3e-01	3.3e-01
3	7.0e-02	6.9e-02
4	2.6e-03	2.6e-03
5	4.0e-06	4.9e-06
6	4.2e-11	1.2e-06
7	0.0e+00	1.2e-06
8	0.0e+00	1.2e-06

$f(\pm i) = \pm i\alpha$. In [7], we showed that

$$\|f'\|_\infty = |f'(\pm 1)| = \frac{\alpha^2}{2\pi} e^{\pi^2/4\alpha}.$$

This is an example of the severe ill-conditioning of the conformal mapping problem due to the elongated shape known as the "crowding phenomenon"[35], since images of points at the ends of the ellipse under f^{-1} are crowded together on the unit circle exponentially in the aspect ratio of the domain as $\alpha \downarrow 0$. For α approaching about 0.2 a large number of Fourier points N are required to achieve any resolution near the ends of the ellipse, if, indeed, the method converges at all; see Figures 15 and 16. For "pinched" domains, such as the inverted ellipses above, the crowding is generally algebraic in $1/\alpha$. Note that this ill-conditioning is due to overall shape and not to the presence of corners or high curvature, as discussed in [7], and represents a severe limitation on the use of Fourier series and the unit disk as a computational domain; see, e.g., [11] for an alternative. This ill-conditioning has limited the use of these methods for applications, such as the computation of breaking waves [34] or Rayleigh-Taylor instabilities [35], where highly elongated geometries evolve. In this sense, methods mapping from the physical domain to the disk are much more robust; see [36, 38].

Example 3. In practice, there may not be an analytic formula defining the boundary. In Figure 5, the boundary is formed by fitting 10 points in the plane distributed around the origin with a periodic cubic spline using $Ns = 100$ points to parametrize the final curve. The Grassmann maps below can also be applied to this example, but the results look much the same. Note that here the level of error can be no better than the accuracy of the cubic spline used to determine the curve.

TABLE 2. Comparison of errors and approximate timings in seconds on a laptop using MATLAB for cubic spline and trigonometric interpolation for the inverted ellipse with $igm = 10$ preliminary Grassmann maps and 10 Newton iterations for Fornberg's method. Interpolation is needed to provide a good initial guess for the trig interpolation parameter.

			trig	interp	spline	interp
α	Ns	N	error	time	error	time
0.4	2000	256	1.2e-04	0.37	1.2e-04	0.06
	2000	512	5.5e-06	0.89	5.5e-06	0.07
	2000	1024	2.3e-08	1.26	1.5e-07	0.07
	2000	2048	1.3e-09	2.59	2.3e-07	0.08
	2000	4096	1.3e-09	4.69	2.3e-07	0.11
	4096	4096	6.9e-14	10.09	9.4e-09	0.13
0.2	2000	256	1.0e-04	0.43	1.0e-04	0.07
	2000	512	2.0e-06	0.84	1.7e-06	0.08
	2000	1024	1.5e-06	1.25	6.0e-07	0.08
	2000	2048	1.3e-06	2.55	5.7e-07	0.09
	2000	4096	1.2e-06	4.48	5.7e-07	0.12
	4096	4096	3.4e-09	12.60	3.4e-08	0.16
0.1	2000	256	2.4e-03	0.39	2.5e-03	0.07
	2000	512	2.3e-04	0.74	2.3e-04	0.08
	2000	1024	7.2e-05	1.49	4.4e-06	0.08
	2000	2048	7.9e-05	2.77	1.3e-06	0.09
	2000	4096	6.6e-05	5.46	1.3e-06	0.15
	4096	4096	7.9e-06	10.13	3.6e-07	0.16

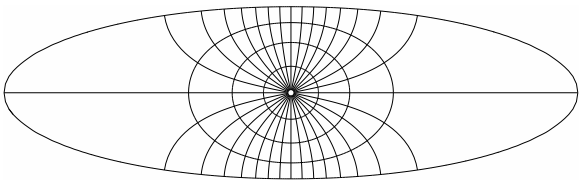

FIGURE 4. Ill-conditioned map: $\alpha = 0.3$ ellipse using $N = 2048$ with standard initial guess. $Ns = 2000$ spline points were used, but an analytic parametrization yields similar results. 11 Newton iteration gives an error in the successive iterates of 0 to machine precision. With $N = 1024$, small oscillations can be seen near ± 1. Results with two crescent maps are slightly worse.

2.4. **Grassmann's method.** This section reports several numerical examples for simply connected domains with Grassmann's routine [17], a method for producing a composition of elementary maps converging to the Riemann map to the unit disk. The domain Ω to be mapped must be normalized so that it is contained in the unit disk with $0 \in \Omega$ and at least two boundary points of modulus 1. The elementary maps gradually expand the domain conformally to fill the disk producing a nearly circular domain. These maps are in the class of osculation maps g_i and their composition $g_k \circ \cdots \circ g_2 \circ g_1$ converges to the Riemann map at an very slow asymptotic rate of $O(1/k)$. However, they exhibit fast initial convergence as observed by Grassmann and others and analyzed by Henrici [23, 24]. In our examples below, $k \leq 10$ is generally sufficient to produce a nearly circular domain which can be mapped by Fornberg's method.

We illustrate the behaviour of the Grassmann maps on our two test cases. We will compare the use of inverted Grassmann maps composed with Fornberg's map to the near-circular domain with the computation of the Fornberg map directly to the domain. The first example applies the

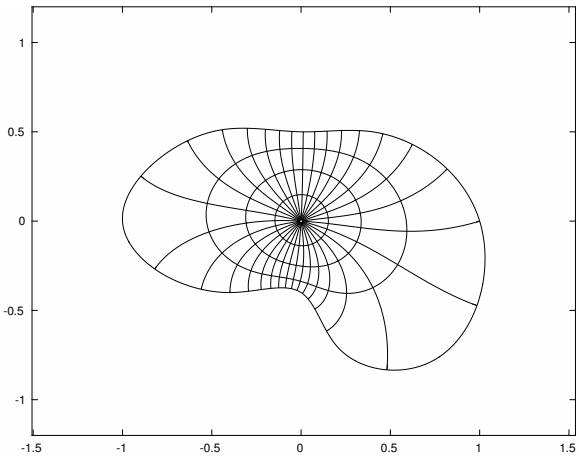

FIGURE 5. Fornberg map to a curve with defined by $Ns = 100$ spline points using $N = 256$.

Grassmann method to map an inverted ellipse to a nearly circular curve after several iterations. The second example is the map to an ellipse. Results for other examples from [7], such as the Cassini oval and the arctanh region yield similar results. Fornberg maps to near circles produced by preliminary Grassmann maps don't require special initial guesses.

We consider two of Grassmann's elementary mappings, the "circle" or "crescent mapping" and the "Koebe mapping". Grassmann used a third elementary map based on the Koebe function, $k(z) = z/(1-z)^2$ and Porter [40] suggested other ways to accelerate the initial convergence. However, we do not need these alternatives here.

To choose between the two maps at each iteration, we first find the point of modulus A on the boundary of Ω closest to 0. Next, we find the circle K tangent to the boundary of Ω at that point. Ω is rotated so that the point of modulus A goes to $-A$. If the unit disk containing Ω and the circle K intersect, they form a crescent containing Ω. The crescent can be mapped to unit disk, expanding the point of modulus A to the unit circle.

If K does not intersect the unit disk, then we use the Koebe mapping. Again, Ω is rotated so that the nearest point to the origin maps to $-A$. Then $-A$ is mapped to the origin by a self-map of the disk, a square root is taken, and a self-map of the disk maps the origin to $-\sqrt{A}$. Since $0 < A < 1$, we have $-\sqrt{A} < -A$, expanding the boundary out toward the unit circle.

2.4.1. *Grassmann map calculation.* We give a short review of some of the details in [17]. Let $z_j, j = 1, \ldots, Ns$ be points on the boundary Γ of Ω. Let $z_{i_0} \in \Gamma$ be the point on the boundary of Ω nearest to 0. Let $i_1 = i_0 - 1$ and for $j \neq i_0, i_1$

$$A_j = \frac{z_j - z_{i_0}}{z_j - z_{i_1}} \left| \frac{z_j - z_{i_1}}{z_j - z_{i_0}} \right| = e^{i\alpha_j},$$

where $-\pi < \alpha_j < \pi$. The approximate tangent circle K will be the circle through z_j, z_{i_0}, z_{i_1} such the Im $\mathrm{A_j} = \sin \alpha_\mathrm{j}$ is smallest. The calculations of the radius R and the center C of circle K are given by

$$R = \frac{1}{2} \frac{|z_{i_0} - z_{i_1}|}{|\text{Im } A_j|} \qquad \text{and} \qquad C = \frac{1}{2} \left[z_{i_0} + z_{i_1} + i(z_{i_0} - z_{i_1}) \frac{\text{Re } A_j}{\text{Im } A_j} \right].$$

If Im $A_j < 0$, i.e., $\alpha_j < 0$, we delete the interior of K. Otherwise, if Im $A_j > 0$, i.e,. $\alpha_j > 0$, we delete the exterior of K. We multiply the region Ω and circle K by $C/|C|$ so that the center lies on the x-axis. If K intersects the unit circle in two points we will use the crescent map. Otherwise, we use the second Koebe routine. The intersection points between K and unit circle are given by

$$x := \text{Re } Z_1 = [(C+R)(C-R)+1]/(2C) \qquad \text{and} \qquad \text{Im } Z_1 = \sqrt{1-x^2}$$

where Z_1 and $\overline{Z_1}$ are the calculated points of intersection.

2.4.2. *Circle or crescent map.* Let K be the disk that intersects the boundary of the simply connected curve Ω. The crescent map will be constructed by the composition of the following elementary mappings. Let Z_1 and $\overline{Z_1}$ be the intersection points between K and Ω from the previous calculations, and let z_{j_0} be the intersection of circle K and the real axis. The first elementary transformation of the crescent map is the Möbius transformation that will map the crescent to a wedge with angle ϕ,

$$z \to T(z) = t_m \frac{z - Z_1}{z - \overline{Z_1}} \qquad \text{where} \qquad t_m = \frac{z_{j_0} - \overline{Z_1}}{z_{j_0} - Z_1}.$$

The second elementary transformation maps to the half plane by raising the first elementary transformation to the power π/ϕ

$$T(z) \longrightarrow T(z)^{\pi/\phi}.$$

Finally, the half plane is mapped to the disk by the elementary transformation

$$T(z)^{\pi/\phi} \to g_c(z) = t_{m_1} \frac{T(z)^{\pi/\phi} - t_0}{T(z)^{\pi/\phi} - \overline{t_0}}$$

$$\text{where} \qquad t_0 = T(0)^{\pi/\phi} \quad \text{and} \quad t_{m_1} = \frac{T(1)^{\pi/\phi} - \overline{t_0}}{T(1)^{\pi/\phi} - t_0}.$$

Therefore, the crescent map will be the composition of the all three elementary transformations,

$$z \to T(z) = t_m \frac{z - Z_1}{z - \overline{Z_1}} \longrightarrow T(z)^{\pi/\phi} \to g_c(z) = t_{m_1} \frac{T(z)^{\pi/\phi} - t_0}{T(z)^{\pi/\phi} - \overline{t_0}}.$$

Figure 6 shows the result of a crescent map applied to an ellipse, where the center of the circle tangent to the ellipse at the point nearest the origin lies to the right of the origin. Figure 7 shows the result of a crescent map applied to an inverted ellipse, where the center of the circle tangent to the inverted ellipse at the point nearest the origin lies to the left of the origin.

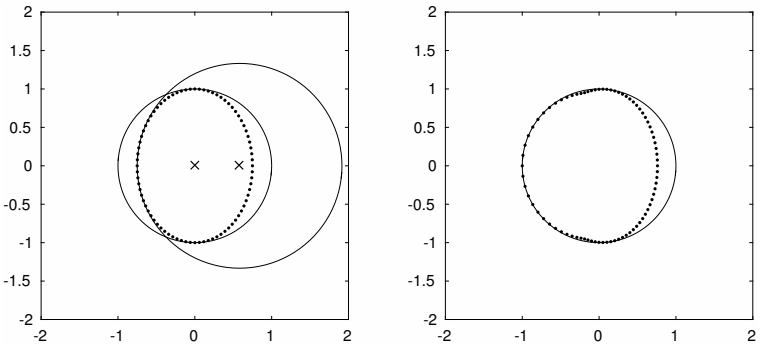

FIGURE 6. One crescent map applied to an ellipse with $\alpha = 0.75$. The 'X's on the left figure mark the centers of the unit and tangent circles.

2.4.3. *Koebe map.* This map is based on the function used in the proof of the Riemann Mapping Theorem; see [1, 24]. It moves the boundary to the unit circle more slowly than the crescent map, but it can be applied to any boundary. Here the tangent circle K is entirely in the unit disk where z_{i_0}, the point closest to 0, is rotated to $-A = -|z_{i_0}|$. R is the radius and C is the center of the circle tangent to the boundary at $-A$. This means $C < 0$ and $R + |C| < 1$. We map the unit disk slit along negative x-axis to $-P = -(C + \gamma R)$ where $0 < \gamma < 1$ and $-1 < -P < 0$ since $0 \in \Omega$. Here we use $\gamma = 0.9$, so that square roots aren't taken on the boundary. The first elementary mapping is to map the point $-P$ to the center 0 by a self-map of the unit disk,

$$z \quad \longrightarrow \quad w = \frac{z + P}{1 + Pz}.$$

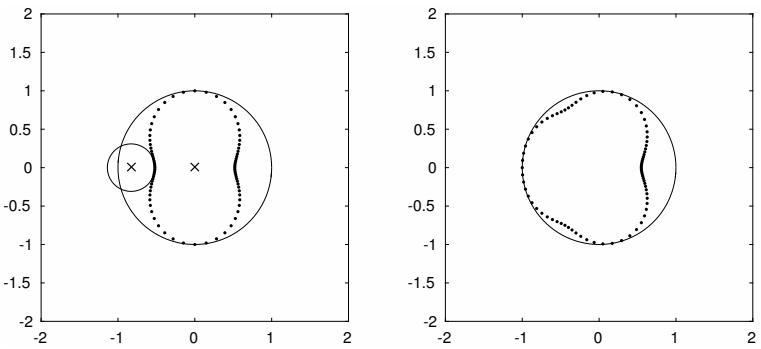

FIGURE 7. One crescent map applied to an inverted ellipse with $\alpha = 0.52$.

The next elementary transformation is the square root that maps the slit to the half disk,

$$w \longrightarrow \sqrt{w},$$

and the last transformation to the desired shape is

$$\sqrt{w} \quad \longrightarrow \quad \frac{\sqrt{w} - \sqrt{P}}{1 - \sqrt{w}\sqrt{P}}.$$

The Koebe map will be the composition of the all three elementary transformations,

$$z \quad \longrightarrow \quad w = \frac{z + P}{1 + Pz} \quad \longrightarrow \sqrt{w} \quad \longrightarrow \quad g_k(z) = \frac{\sqrt{w} - \sqrt{P}}{1 - \sqrt{w}\sqrt{P}}.$$

Note that $-P \to 0 \to -\sqrt{P} < -P$ and so that the boundary near $-A \approx -P$ will be moved toward the unit circle. Figure 8 illustrates the steps in the construction for an inverted ellipse where the tangent circle does not intersect the unit circle and the crescent map cannot be used.

2.4.4. *Inverse Crescent Map.* The inverse of the crescent mapping uses the following conformal mapping transformations.

$$z \to w = \frac{\overline{t_0} z - t_0 t_{m_1}}{z - t_{m_1}} \to w^{\phi/\pi} \to \frac{\overline{Z_1} w^{\phi/\pi} - Z_1 t_m}{w^{\phi/\pi} - t_m}$$

2.4.5. *Inverse Koebe Map.* The inverse of the Koebe mapping uses the following conformal mapping transformations.

$$z \to w = \frac{z + \sqrt{P} z}{1 + \sqrt{P}} \to w^2 \to g^{-1} = \frac{w^2 + P}{1 + P w^2}$$

Example 4 (Grassmann iterations)**.** Some iterations of the Grassmann maps applied to an inverted ellipse, Example 1 with "thinness" $\alpha = 0.2$, are shown in Figures 9 and the rate of convergence of the boundary to the unit circle for various α is illustrated in Table 3. Note that the initial convergence rate is fast, as discussed in [23, 24, 40]. The resulting distribution of $Ns = 400$ points on the near-circle after $igm :=$ the number of Grassmann maps $= 10$ is shown in Figure 10. The boundary of the nearly circular domain is parametrized by fitting a periodic cubic spline parametrized by chordal arc length, as descibed above, through these points. To increase the overall accuracy more spline points Ns can be mapped at a relatively cheap cost of order $Ns\times$ the number of Grassmann iterations. Examples of other curve families, such as those discussed in [7], have been computed in [2, 4] with similar results.

2.5. **Removing Corners.** In this section, we introduce a method for systematically removing corners. The method is based on the Koebe map above for general curves. An example of a square is used to calculate the error in removing its corners with our Koebe-like method compared to the Schwarz-Christoffel map using SC Toolbox [14], which is highly accurate. See [9, 10, 18, 29, 30, 31, 44] for related papers. The domain Ω is normalized inside the unit disk such that $0 \in \Omega$ and such that none of the corners lie on the unit circle. We apply the following procedure, similar to the

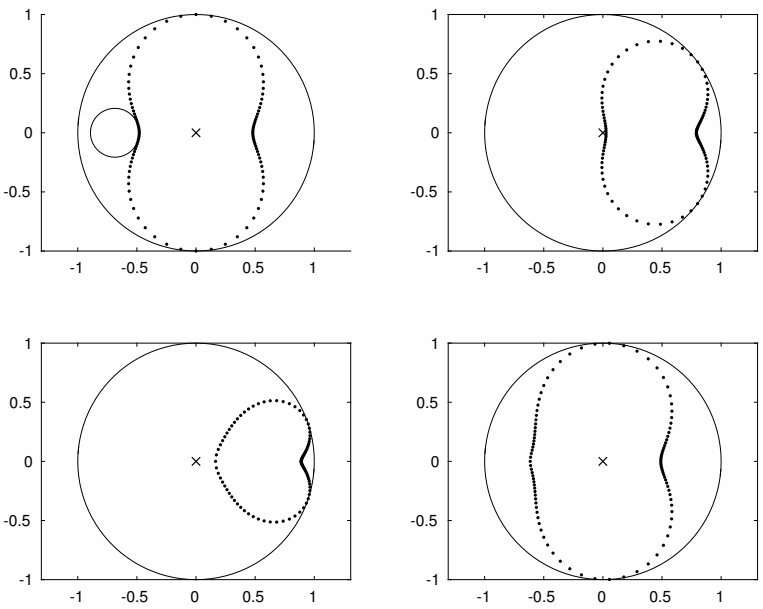

FIGURE 8. Steps for one Koebe map applied to an inverted ellipse with $\alpha = 0.48$. Note that the circle tangent to the boundary at the point nearest the origin does not intersect the unit circle, so that the crescent map cannot be applied. The square root is taken at the origin slightly off of the boundary curve, so that the curve remains smooth.

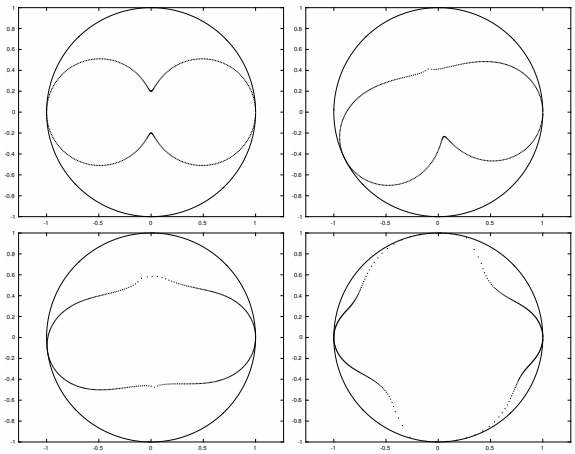

FIGURE 9. Iterations 1, 3, and 6 of Grassmann maps applied to an inverted ellipse with $\alpha = 0.2$; see Table 3.

Koebe map above, successively to each corner. First, we rotate the corner z_k with $|z_k| = A < 1$ to $-A$. Next we apply the following sequence of maps, where $\beta_k \pi$ is the corner angle,

$$z \quad \longrightarrow \quad Z = \frac{z + A}{1 + Az} \quad \longrightarrow W = Z^{1/\beta_k} \quad \longrightarrow \quad w = k(z) = \frac{W - A^{1/\beta_k}}{1 - A^{1/\beta_k} W}.$$

One step of this procedure is shown in Figure 17.

TABLE 3. Convergence of the Grassmann maps (ig) for inverted ellipses, $\alpha = 0.8, 0.4, 0.2, 0.1$, ig = c = circle (crescent)map, ig = k = Koebe map. Note the fast initial convergence, but slow asymptotic convergence. Here $Ns = 400$ and $\gamma = 0.9$.

ig	α	ig	α	ig	α	ig	α
0	.800	0	.400	0	.200	0	.100
c	.804	k	.416	k	.239	k	.150
c	.950	k	.571	k	.449	k	.361
		c	.594	k	.464	k	.388
		c	.770	k	.535	k	.484
		c	.775	c	.563	c	.528
		c	.912	c	.717	c	.704
		c	.912	c	.725	c	.713
		c	.961	c	.885	c	.917
		c	.962	c	.886	c	.918
		c	.968	c	.957	c	.960

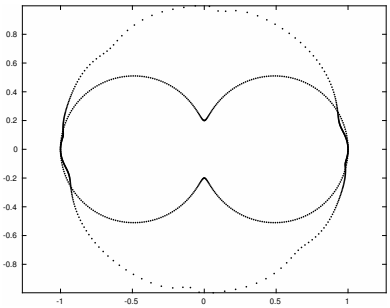

FIGURE 10. Inverted ellipse $\alpha = 0.2$ with $igm = 10$ and $Ns = 400$.

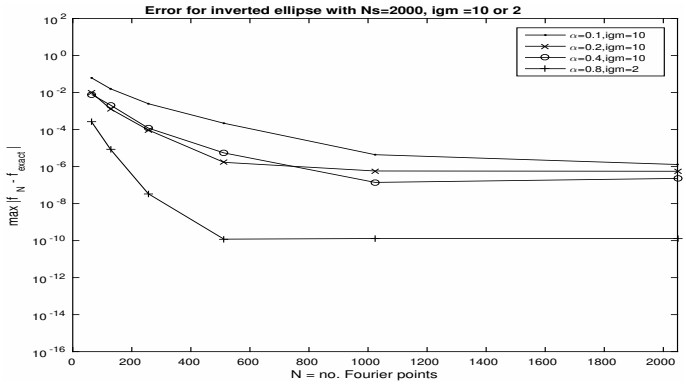

FIGURE 11. Errors for Grassmann maps to inverted ellipse $Ns = 2000$.

Example 5 (Examples and comparison with Schwarz-Christoffel Toolbox)**.** In this section, we give three examples of our corner-smoothing, Koebe-like method. The first is the map from the unit disk to a square, Figures 18. The intermediate Fornberg map to the domain smoothed by four corner-removing maps is displayed in Figure 19. The error is computed in Table 4 by comparison with the map produced by SC Toolbox [14]. Even with $N = 1024$ Fourier points, we only get about 3 digit

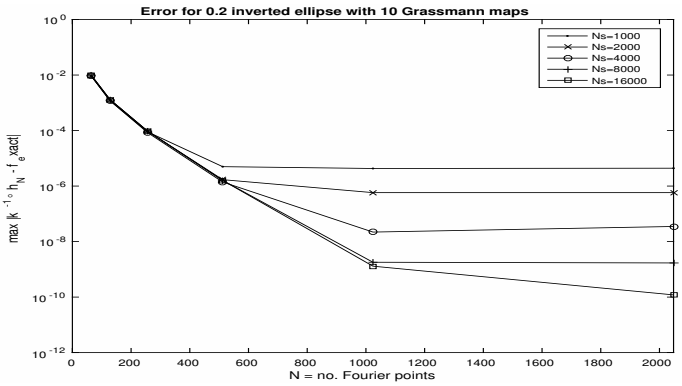

FIGURE 12. Errors for 10 Grassmann maps to inverted ellipse with $\alpha = 0.2$ and various numbers of splines points Ns demonstrating that errors can be made smaller by increasing both N and Ns. Note for fixed Ns the minimum achievable error is fixed for a given domain.

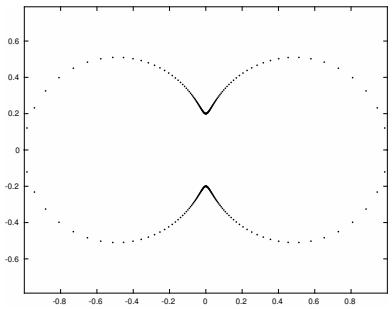

FIGURE 13. Inverted ellipse $\alpha = 0.2$ with $igm = 10$ and $Ns = 400$: distribution of $N = 256$ Fourier points.

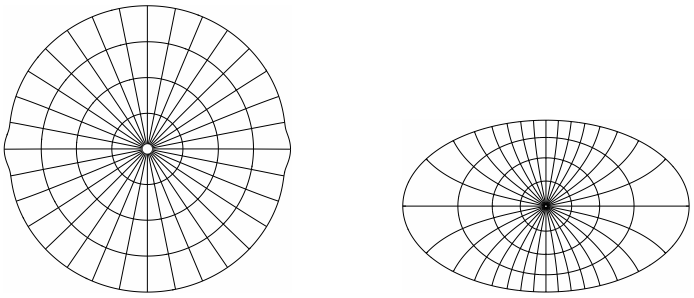

FIGURE 14. Fornberg map for ellipse $\alpha = 0.6, N = 256$ with two preliminary crescent maps to near circle.

accuracy. This is consistent with our other experience computing maps to domains with corners with methods based on Fourier series in [9, 10]. Typically one may see small oscillations of the boundary near the corners. (A careful study of the behaviour of Theodorsen's method, a Fourier series method, combined with techniques for smoothing the series, such as Lanczos smoothing, for domains with corners is given in [18].) A map to a polygon with 5 corners, including a re-entrant

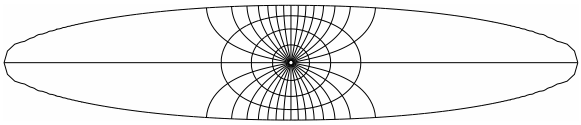

FIGURE 15. Ill-conditioned map: $\alpha = 0.2$ ellipse using $N = 32,768$ with standard initial guess. $Ns = 4000$ spline points were used, but analytic parametrization yields similar results. 6 Newton iteration gives error in successive iterates of $1.0 \cdot 10^{-4}$. Note the poor resolution near ± 1.

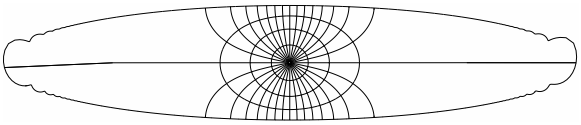

FIGURE 16. The map to an ellipse with $\alpha = 0.2$ is computed by the Fornberg map to near circle composed with 2 inverted crescent maps, $N = 32,768$. $Ns = 4000$ spline knots were used.

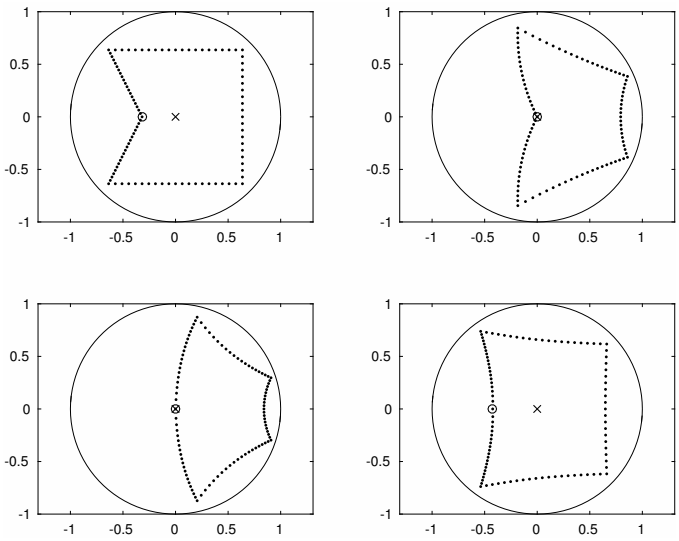

FIGURE 17. The steps for smoothing a corner: The domain is placed slightly inside of the unit disk and each corner is successively rotated to the negative real axis and mapped to the origin with a Möbius map of the disk taking the corner to the origin. The corner is smoothed with a power map, and the origin is mapped back to the negative real axis.

corner, is shown in Figure 20. Also, a map to a crescent is shown in Figure 21. In this case the exact map is known and the accuracy is only about 2 digits. This is a simple example of a curvilinear domain with corners. SC Toolbox is restricted to polygonal domains. However, a "generalization" of the Schwarz-Christoffel transformation to exterior curvilinear polygons was considered in [10], but did not give high accuracy. To treat curvilinear domains with high accuracy, methods which map to the disk and can refine the mesh in the target domain near the corners should be used; see,

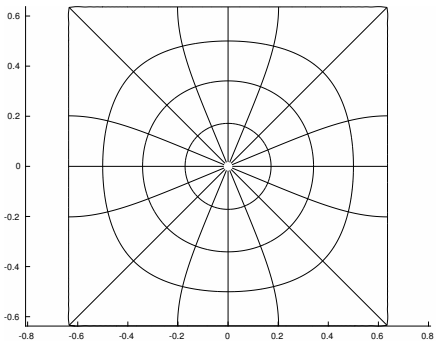

FIGURE 18. Inverses of corner smoothing maps composed with Fornberg's map for a square.

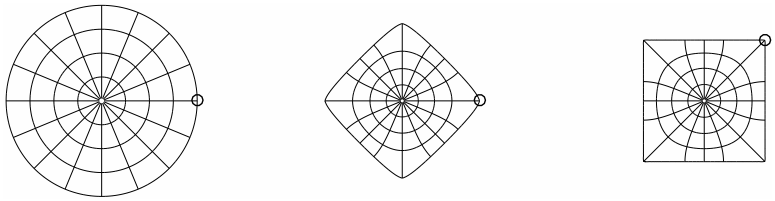

FIGURE 19. Sequence of maps from the unit disk to smoothed domain to a square $N = 1024$ for Fornberg's method and $Ns = 200$ points per side.

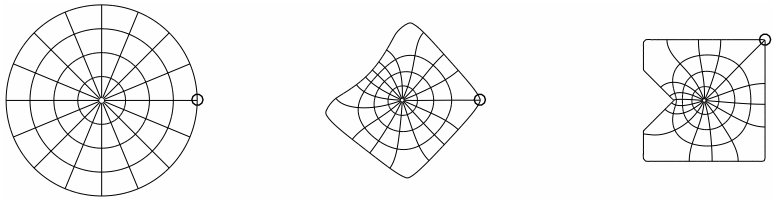

FIGURE 20. Sequence of maps from the unit disk to a smoothed domain to a polygon with $N = 1024$ for Fornberg's method.

e.g., [36] and also [39, Remark 1.5.3] and [19, 20] for alternative methods which can treat corners and even cusps using singular functions or adaptive methods.

TABLE 4. The calculated error of the Koebe-like corner-removing method compared with the exact map to the square given by SC Toolbox for several values of N for the Fornberg map.

N	Error
64	.1497
128	.0697
256	.0246
512	.007
1024	.0019

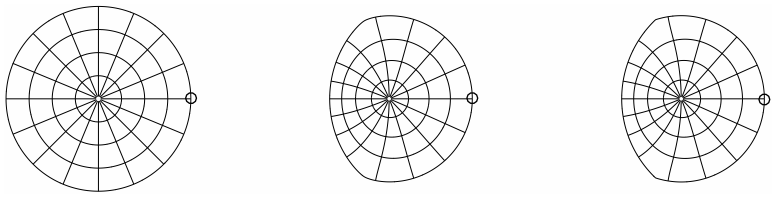

FIGURE 21. Sequence of maps from the unit disk to a smoothed domain to a crescent with $N = 256$ for Fornberg's method. The exact map to the crescent is known The error using Fornberg's method is between 10^{-4} to about $1.5 \cdot 10^{-2}$ near the prevertices and changes very little with increased N and Ns.

3. **Multiply connected domains.** In order to clarify the existence and uniqueness for the conformal map $w = f(z)$ for the multiply connected case, let us first consider unbounded regions containing infinity. Let f be conformal map from the complement, D, of m closed nonintersecting disks, D_k, onto a region Ω which is exterior to m nonintersecting smooth Jordan curves, $\Gamma_k, 1 \leq k \leq m$. The following theorem (actually stated for f^{-1} in [24, 17.1b]) establishes the existence and uniqueness of the circle map under suitable normalization conditions.

Theorem 3.1. *Let Ω be a region of connectivity $m \geq 2$ in the extended complex plane such that $\infty \in \Omega$. Then there exists a unique circular region D of connectivity m and a unique one-to-one analytic function f in D satisfying*

$$f(z) = z + O(1/z) \quad for \quad z \approx \infty,$$

such that $f(D) = \Omega$.

3.1. **Extension of Fornberg's method to exterior multiply connected domains.** The details of this method are presented in [3]. We review them briefly here. Boundaries of disks D_k are the circles $C_k : c_k(\theta) := z_k + \rho_k e^{i\theta}$ and $C = C_1 + \cdots + C_m$. The target boundary of Ω is $\Gamma = \Gamma_1 + \cdots + \Gamma_m$, where the Γ_k are (smooth) curves parametrized by S, e.g., arclength, $\Gamma_k : \gamma_k(S)$. f extends smoothly to the boundary $f(C_k) = \Gamma_k$. To compute the map, we must find the boundary correspondences $S = S_k(\theta)$ and conformal moduli z_k, ρ_k such that

$$f(z_k + \rho_k e^{i\theta}) = \gamma_k(S_k(\theta)), 1 \leq k \leq n,$$

where f is analytic and $f(z) = z + O(1/z), z \approx \infty$. Therefore,

$$f(z) = z + \sum_{k=1}^{m} \sum_{k=j}^{\infty} a_{k,j} \left(\frac{\rho_k}{z - z_k} \right)^j.$$

As in the simply connected case, we will linearize the problem about the current guesses for the boundary correspondences and centers and radii and use a Newton-like iteration. For an initial guess $S_k(\theta)$ and 2π periodic correction $U_k(\theta)$, we use the following linearization for $U_k(\theta)$

$$\gamma_k(S_k(\theta) + U_k(\theta)) \approx \gamma_k(S_k(\theta)) + \gamma_k'(S_\nu(\theta))U_k(\theta).$$

For an initial guess of z_k and ρ_k with corrections δz_k and $\delta \rho_k$,

$$(f + \delta f)(z_k + \delta z_k + (\rho_k + \delta \rho_k)e^{i\theta}) \approx (f + \delta f)(z_k + \rho_k e^{i\theta}) + f'(z_k + \rho_k e^{i\theta})(\delta z_k + \delta \rho_k e^{i\theta}).$$

The above approximations gives

$$(f + \delta f)(z_k + \rho_k e^{i\theta}) = \gamma_k(S_k(\theta)) + \gamma_k'(S_k(\theta))U_k(\theta) - f'(z_k + \rho_k e^{i\theta})(\delta z_k + \delta \rho_k e^{i\theta}).$$

Requiring the functions to be boundary values of a function analytic in D gives a linear system for the unknown Newton updates $U_k, \delta z_k, \delta \rho_k$ denoted by $\underline{U}$, of the form,

$$A\underline{U} = \underline{b},$$

where A is a symmetric positive definite matrix of the form identity plus a low rank operator. The system can be solved efficiently by the conjugate gradient method, as in the simply connected case, except that the matrix-vector multiplication now costs $O((mN)^2)$ operations instead of $O(N \log N)$.

The $i+1$st Newton updates are then,

$$\begin{aligned} S_k^{i+1} &= S_k^i + U_k^i \\ z_k^{i+1} &= z_k^i + \delta z_k^i \\ \rho_k^{i+1} &= \rho_k^i + \delta \rho_k^i. \end{aligned}$$

Example 6 (Preliminary Grassmann maps for multiply connected domains)**.** In this section, we apply Grassmann maps to multiply connected exterior domains and compose them with the Fornberg maps. Figure 22 shows a domain of connectivity $m = 4$ mapped with Grassmann maps to produce the near circles. The domains are successively inverted and the Grassmann maps for the interior are used to produce the near circles. The extension of Fornberg's method to the exterior multiply connected case [3] is used to compute the map from the exterior of $m = 4$ circles to the exterior of the near circles and then the inverse Grassmann maps map to the original domain. The differences in the successive iterates of the Fornberg method are shown in Table 5 and indicate that the discrete problems is solved accurately. Fornberg's method to map directly to this domain did not converge using the standard initial guess. For the domain in Figure 23, both the direct map to the domain and the map computed with Grassmann maps converged.

TABLE 5. Convergence of successive Newton-iteration errors $\|S^{i+1} - S^i\|_\infty$ at the Fourier points for the Fourier series map to the the near-circular region of connectivity $m = 4$ in Figure 22 for $N = 128, 256$. Note that the convergence rate is nearly independent of N. (The number of conjugate gradient iterations to solve the inner linear systems was fixed at 30.)

Newton iterations	$N = 128$	$N = 256$
1	1.6e+00	3.3e+00
2	7.5e-01	1.5e-00
3	1.3e-02	2.5e-02
4	5.5e-04	1.5e-03
5	5.6e-06	5.7e-06
6	3.7e-08	1.5e-08
7	3.4e-10	2.6e-11
8	2.2e-12	1.0e-13
9	3.1e-14	5.6e-14
10	1.8e-14	2.7e-14

In Figure 24 the Fornberg map is composed with successive applications of our corner smoothing method to produce the map to the exterior of $m = 3$ rectangles. Table 7 shows the convergence of the successive iterates for near circular domains resulting from domains with corners.

4. **Karman-Trefftz transformations and potential flow.** A popular method for removing a single corner on the boundary curve of a domain exterior to the curve and containing ∞ is the Karman-Trefftz transformation. This has been used often for computing potential flow over the exterior of a multi-element airfoil [21]. If the exterior angle is then $\beta\pi$, the Karman-Trefftz transformation is given by

$$\frac{\zeta - \zeta_1}{\zeta - \zeta_2} = \left(\frac{z - z_1}{z - z_2}\right)^\beta,$$

where z_1, the corner at the trailing edge, maps to ζ_1 and z_2, a point chosen interior to the curve near the leading edge, maps to ζ_2. Then

$$k(z) = \zeta = \left(\zeta_1 - \zeta_2 \left(\frac{z - z_1}{z - z_2}\right)^{1/\beta}\right) / \left(1 - \left(\frac{z - z_1}{z - z_2}\right)^{1/\beta}\right)$$

and its inverse is

$$k^{-1}(\zeta) = z = \left(z_1 - z_2 \left(\frac{\zeta - \zeta_1}{\zeta - \zeta_2}\right)^{\beta}\right) / \left(1 - \left(\frac{\zeta - \zeta_1}{\zeta - \zeta_2}\right)^{\beta}\right).$$

TABLE 6. Some typical sample timings for map to regions in Figure 22 with $m = 4$. The number of Newton iterations are fixed at 10 and the number of conjugate gradient iterations are fixed at 30. For $m = 2$, we map to the exterior of the upper and right inverted ellipses in Figure 22. We use $igm = 8$ Grassmann maps, but times are similar with no preliminary maps. The dominant operation count is the $O((mN)^2)$ matrix-vector multiplication for solving the conjugate gradient solution for the inner linear systems for the Fornberg map.

Ns	N	time (m=4)	time (m=2)
200	128	1.45	0.77
200	256	3.65	1.64
200	512	15.92	3.36
400	128	1.71	0.73
400	256	3.54	1.11
400	512	15.66	3.28
800	128	1.56	0.81
800	256	3.62	1.16
800	512	15.73	3.30

The application of $k(z)$ to the airfoil usually results in a nearly circular set of point which we fit with our periodic cubic spline routine parametrized by chordal arclength, as in the application of the osculation maps. For the multiply connected case, the Karman-Trefftz transformation can be applied successively to the images of the m airfoils to produce a map $k = k_m \circ \cdots \circ k_2 \circ k_1$ from the domain Ω bounded by airfoils to the domain $k(\Omega)$ bounded by nearly circular, smooth curves. Note that each of these maps k_i must be applied to all of the curves at each step. Fornberg's method for exterior multiply connected domains [3] can then be used to compute a Laurent series map h from a conformally equivalent domain D exterior to m disks to $k(\Omega)$. The Karman-Trefftz maps k_i can be explicitly inverted. The final conformal map f from the circle domain D to the domain Ω exterior to the m airfoils can be represented as a composition,

$$f = k^{-1} \circ h = k_1^{-1} \circ k_2^{-1} \circ \cdots k_m^{-1} \circ h.$$

The procedure is illustrated by two examples below, Figure 26 for a single Joukowski airfoil and Figure 28 for $m = 2$ cosine curves. An `X` marks the $z_1, z_2, \zeta_1, \zeta_2$ for each (transformed) domain. We compute the streamlines about the airfoils by adding circulation to streaming flow in order to satisfy the Kutta-Joukowski condition at the trailing edge, as in [21, 45]. A more complete discussion of this procedure will be given in future work.

Example 7. The first example is the map to the exterior of a Joukowski airfoil Figure 26. This is a well-known case where the map from the exterior of a circle to the exterior of an airfoil with given trailing edge angle is known explicitly; see [33]. Specifically, the map used here to an airfoil with interior trailing edge angle 0.15π radians is given by the sequence of maps,

$$\begin{aligned} z &= (1+h)\sqrt{(1+b^2)}\exp(i(\theta+\theta_1)) - h + (1+h)bi \\ Z &= (z-1)/(z+1) \\ W &= Z^{1.925} \\ w &= (2+2*W)/(1-W), \end{aligned}$$

where $b = 0.2, h = 0.2, \theta_1 = \tan^{-1}(-b)$. Figure 25 illustrates the case where $Ns = 101$ points, equally spaced in θ, are distributed about the airfoil and mapped with $k(z)$ to a smooth domain. We deliberately do not just invert the Joukowski map to the circle in order to have an exact test case. The errors between the exact Joukowski map and $k^{-1} \circ h$ for increasing values of N and Ns are given in Figure 27. Note that the error can be made as small as we please, since the preimage of the one vertex at the trailing edge can always be made to be a Fourier point. This is not possible, in general, for connectivity greater than one.

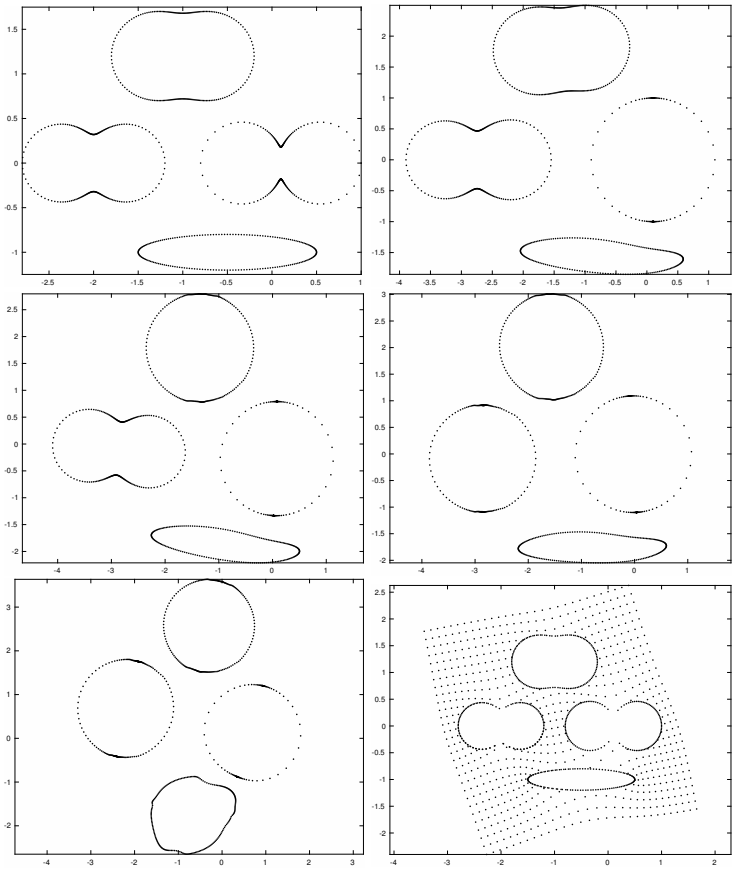

FIGURE 22. Fornberg composed with Grassmann maps for exterior of $m = 4$ curves - 3 inverted ellipses and an ellipse with $N = 128, igm = 8, Ns = 200$. The Fornberg map directly to the domain did not converge.

Example 8. The second example is the domain exterior to two cosine airfoils. The boundaries are given by

$$\gamma(\sigma) = -\cos(K\sigma)e^{i\sigma}, \qquad -\frac{\pi}{2K} \le \sigma \le \frac{\pi}{2K}$$

with a trailing edge interior angle $\frac{\pi}{K}$ and $K = 2$. We apply this to a distribution of 400 points along the cosine curve with angle $\beta\pi = 2\pi - \pi/K$, and $1/\beta = \frac{K}{2K-1}$.

Table 7 lists the maximum error between the successive iterations of the boundary correspondence functions S_1^i and S_2^i, illustrating the near quadratic convergence of Fornberg's method. (Recall that this does not give the discretization error which depends on N, but only the accuracy of the solution to the discrete problem. This rate is independent of N.) In, e.g., [21] and earlier work, linearly convergent Fourier series methods, such as those of Theordorsen or Timman/James [27] for simply connected domains applied successively to each boundary, were used for the maps to the smoothed domains; see [24] for a presentation of these methods and [9] for comparisons with the methods of Fornberg and Wegmann for simply connected regions. In [9], a discretization error of 10^{-4} was achieved with this approach for the simply connected case with $N = 256$.

5. **The bounded, multiply connected case.** A version of our Fourier series method for mapping to bounded multiply connected regions with smooth boundaries has been developed in [12].

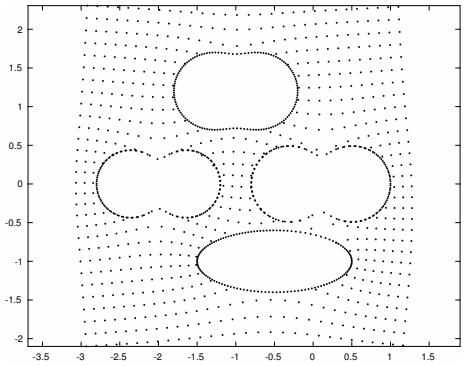

FIGURE 23. This domain is the same as the domain above, except that the thin ellipse and inverted ellipse are changed from $\alpha = 0.2$ to $\alpha = 0.4$. Both the Fornberg map directly to the domain and composed with preliminary Grassmann maps converged for this case with $N = 128, Ns = 200, igm = 0$ or 8.

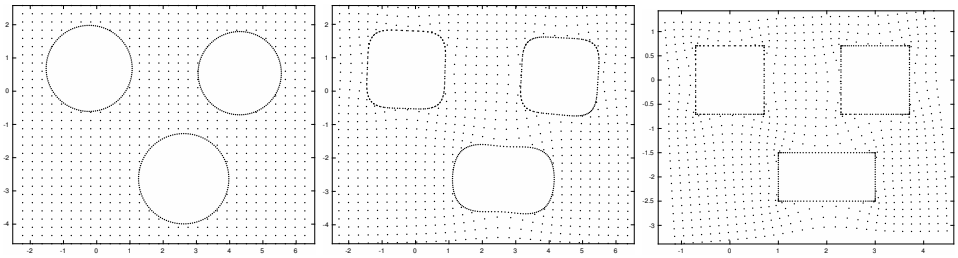

FIGURE 24. Fornberg is composed with corner smoothing maps to the exterior of $m = 3$ rectangles with $N = 128$ and $Ns = 50$ points per side.

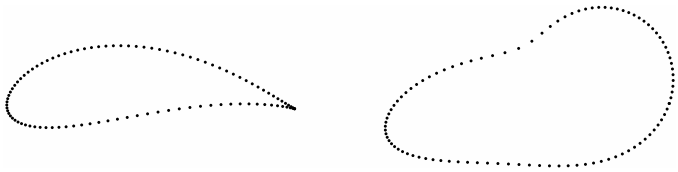

FIGURE 25. Joukowski airfoil smoothed by Karman-Trefftz map.

We have not done much testing of this method with explicit preliminary maps, but we expect the results to be much the same as the unbounded case, above. Figure 29 shows the map to the interior of a diamond with elliptical holes, where the corners have been smoothed using our Koebe-like method. The straight sides are well represented, but it is again difficult to resolve the corners very sharply.

6. **Concluding remarks.** The results of our computations show that preliminary explicit maps are marginally useful and lead to somewhat more robust methods. An accurate initial guess is easily given for the near-circular regions in both the simply and the multiply connected cases. However, the coding becomes somewhat complicated, especially in the multiply connected case, and accuracy can be lost due to the necessity of parametrizing the nearly circular or smoothed boundaries with curves of lower regularity, such as cubic splines. If the original curves are given by

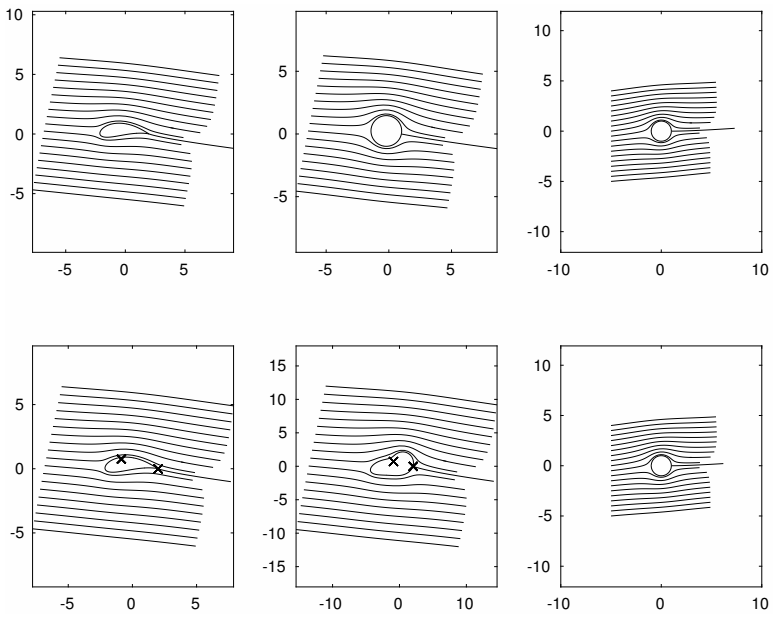

FIGURE 26. Joukowski map and $k^{-1} \circ h$.

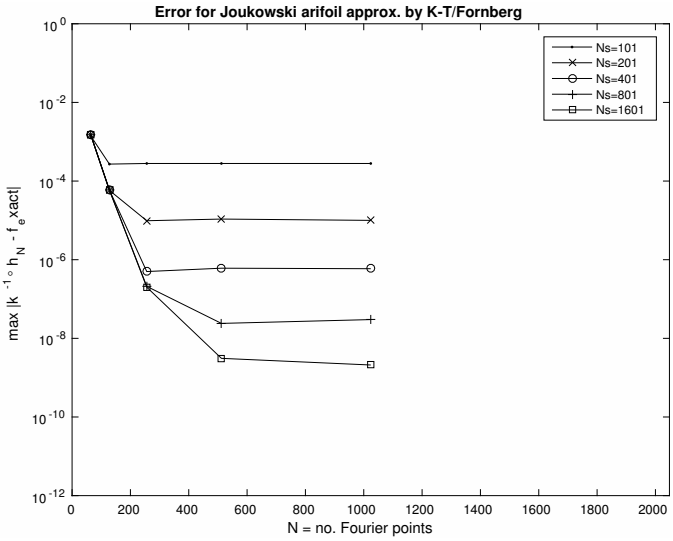

FIGURE 27. Error for Joukowski map and $k^{-1} \circ h$.

spline fits to a finite number of points defining the boundary, the accuracy will be limited from the start. For domains with corners only 3 or 4 digit accuracy can be expected when composing corner smoothing with series methods, except in special cases such as a single airfoil. In future work we plan to compare our results with linearly convergent projection methods described in [41, 42, 44] which can be applied directly to regions with corners. Also, more comparison with Wegmann's Newton-like methods [44] based on solving Riemann-Hilbert problems would be useful and some comparsions were given in [3]. However, we do not expect any significant advantages overall

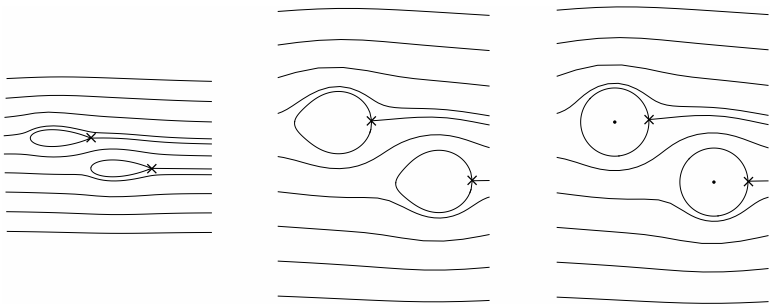

FIGURE 28. Streamlines for potential flow over two cosine airfoils with using the Karman-Trefftz transformation $k, k^{-1} \circ h$, composed with the extension of Fornberg's method for connectivity 2 and $N = 128$. Circulation is computed so that the Kutta condition is satisfied at the trailing edges.

TABLE 7. Convergence of successive Newton-iteration errors $\|S^{i+1} - S^i\|_\infty$ at the Fourier points for the Fourier series map to the the near-circular regions for examples with corners in Figures 24, 26, and 28.

Newton iterations	3 rectangles $N = 128, Ns = 201$	Joukowski airfoil $N = 256, Ns = 101$	Two cosine airfoils $N = 128, Ns = 101$
1	2.3e+01	1.0e+00	3.4e+00
2	2.3e+01	3.0e-01	3.0e-01
3	3.1e+00	2.3e-02	3.0e-03
4	1.0e+00	1.2e-04	1.6e-05
5	5.2e-01	2.1e-09	3.4e-08
6	6.4e-02	5.4e-10	1.1e-10
7	6.9e-03	5.4e-10	3.3e-13
8	1.2e-04	5.4e-10	1.7e-15
9	1.9e-06	5.4e-10	4.1e-15
10	4.0e-08	5.4e-10	9.7e-15
11	6.2e-10		
12	1.3e-11		
13	1.8e-13		
14	1.6e-14		

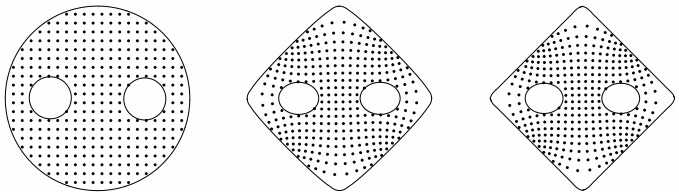

FIGURE 29. The map from the interior of the unit disk (left) with two circular holes to the interior of a diamond (right) with two elliptical holes by smoothing corners on the diamond and using $N = 256$ Fourier points for the map to the smooth region (middle).

(except that the Newton-like methods are faster), since these methods are all based on Fourier series. Also, we plan more complete experiments on computations of potential over airfoils.

Acknowledgments. We thank the referees for several comments and corrections that led to improvements to the paper.

REFERENCES

[1] L. Ahlfors, *Complex Analysis, third edition*, McGraw-Hill, New York, 1979.

[2] M. Badreddine, *Comparison of Some Numerical Conformal Mapping Methods for Simply and Multiply Connected Domains*, Ph.D dissertation, Wichita State University, 2016.

[3] N. Benchama, T. DeLillo, T. Hrycak, and L. Wang, A simplified Fornberg-like method for the conformal mapping of multiply connected regions– comparisons and crowding, *J. Comput. Appl. Math.*, **209** (2007), 1–21.

[4] T. K. DeLillo, *A Comparison of Some Numerical Conformal Mapping Methods*, PhD dissertation, Courant Institute, NYU, 1985.

[5] T. K. DeLillo On the use of numerical conformal mapping methods in solving boundary value problems for the Laplace equation, in *Advances in Computer Methods for Partial Differential Equations-VII*, eds. R. Vichnevetsky, D. Knight, and G. Richter, Seventh IMACS Symposium Proceedings, Rutgers University, (1992), 190–194.

[6] T. K. DeLillo, Comparisons of some numerical conformal mapping methods, in *Proceedings of the 14th IMACS World Congress on Computation and Applied Mathematics, Vol. 1,* ed. W. F. Ames, Georgia Institute of Technology, Atlanta, Georgia, (1994), 115–118.

[7] T. DeLillo, The accuracy of numerical conformal mapping methods: a survey of examples and results, *SIAM J. Numer. Anal.*, **31** (1994), 788–812.

[8] T. DeLillo, *Tutorial on Fourier series methods for numerical conformal mapping of smooth domains*, 2014, http://www.math.wichita.edu/~delillo/TD_tutorial.pdf

[9] T. DeLillo and A. Elcrat, A comparison of some numerical conformal mapping methods for exterior regions, *SIAM J. Sci. Stat. Comput.*, **12** (1991), 399–422.

[10] T. K. DeLillo and A. R. Elcrat, Numerical conformal mapping methods for exterior regions with corners, *J. Comput. Phys.*, **108** (1993), 199–208.

[11] T. K. DeLillo, A. R. Elcrat, and J. A. Pfaltzgraff, Numerical conformal mapping methods based on Faber series, *J. Comput. Appl. Math.*, **83** (1997), 205–236.

[12] T. K. DeLillo and E. H. Kropf, A Fornberg-like method for the numerical conformal mapping of bounded multiply connected domains, submitted for publication.

[13] T. DeLillo and J. Pfaltzgraff, Numerical conformal mapping methods for simply and doubly connected regions, *SIAM J. Sci. Comput.*, **19** (1998), 155–171.

[14] T. A. Driscoll and L. N. Trefethen, *Schwarz-Christoffel Mapping*, Cambridge, 2002.

[15] B. Fornberg, A numerical method for conformal mappings, *SIAM J. Sci. Stat. Comput*, **1** (1980), 386–400.

[16] D. Gaier, *Konstruktive Methoden der Konformen Abbildung*, Springer, Berlin, 1964.

[17] E. Grassmann, Numerical experiments with a method of successive approximation for conformal mapping, *ZAMP*, **30** (1979), 873–884.

[18] M. H. Gutknecht, Numerical experiments on solving Theodorsen's intergral equation for conformal maps with the fast Fourier transfomr and various nonlinear iterative methods, *SIAM J. Sci. Stat. Comput.*, **4** (1983), 1–30.

[19] H. Hakula, T. Quach, and A. Rasila, Conjugate function method for numerical conformal mappings, *J. Comput. Appl. Math.*, **237** (2013), 340–353.

[20] H. Hakula, A. Rasila, and M. Vuorinen, Conformal modulus on domains with strong singularities and cusps, *arXiv:* 1501.06765.

[21] N. D. Halsey, Potential flow analysis of multielement airfoils using conformal mapping, *AIAA J.*, **17** (1979), 1281–1288.

[22] J. Heinhold and R. Albrecht, Zur Praxis der konformen Abbildung, *Rend. Circ. Mat. Palermo Ser. 2*, **3** (1954), 130–148.

[23] P. Henrici, A general theory of osculation algorithms for conformal maps, *J. Linear Alg. Appl.*, **52/53** (1983), 361-382.

[24] P. Henrici, *Applied and Computational Complex Analysis, vol. III*, Wiley, New York, 1986.

[25] H.-P. Hoidn, Osculation methods for the conformal mapping of doubly connected regions, *ZAMP*, **33** (1982), 640–652.

[26] W. D. Hoskins and P. R. King, Periodic cubic spline interpolation using parametric splines, *The Computer Journal*, **15** (1972), 282–283.

[27] R. M. James, A general class of exact airfoil solutions, *AIAA J.*, 9 (1972), pp. 574–580.

[28] W. Koppenfels and F. Stallmann, *Praxis der konformen Abbildung*, Springer, Berlin, 1959.
[29] L. Landweber and T. Miloh, Elimination of corners in the mapping of a closed curve, *J. Engrg. Math.*, **6** (1972), 369–375.
[30] R. S. Lehman, Development of the mapping function at an analytic corner, *Pacific J. Math.*, 7 (1957), 1437–1449.
[31] H. Lewy, Developments at the confluence of anaytic boundary conditions, *Univ. of California Publ. in Math.*, **1** (1950), 247–280.
[32] D. E. Marshall, Conformal welding for finitely connected regions, *Comput. Methods Funct. Theory*, **11** (2011), 655–669.
[33] J. H. Mathews and R. W. Howell, *Complex Analysis for Mathematics and Engineering, Sixth edition*, Jones and bartlett, W, C. Brown, 2010. http://mathfaculty.fullerton.edu/mathews/complex.html
[34] D. I. Meiron, S. A. Orszag, and M. Israeli, Applications of numerical conformal mapping, *J. Comput. Phys.*, **40** (1981), 345–360.
[35] R. Menikoff and C. Zemach, Methods for numerical conformal mapping, *J. Comput. Phys.*, **36** (1980), 366–410.
[36] M. Nasser, Fast computation of the circular map, *Comput. Methods Funct. Theory*, **15** (2015), 187–223.
[37] M. Nasser, T. Sakajo, A. Murid, and L. K. Wei, A fast computational method for potential flows in multiply connected coastal domains, *Japan J. Indust. Appl. Math.*, **32** (2015), 205–236.
[38] S. T. O'Donnell and V. Rokhlin, A fast algorithm for the numerical evaluation of conformal mappings, *SIAM J. Sci. Statist. Comput.*, **10** (1989), 475–487.
[39] N. Papamichael and N. Stylianopoulos, *Numerical Conformal Mapping - Domain Decomposition and the Mapping of Quadrilaterals*, World Scientific, Singapore, 2010.
[40] R. M. Porter, An accelerated osculation method and its application to numerical conformal mapping, *Complex Variables*, **48** (2003), 569–582.
[41] W. J. Prosnak, *Computation of Fluid Motions in Multiply Connected Domains,* G. Braun, Karlsruhe, 1987.
[42] W. J. Prosnak, Conformal representation of arbitrary multiconnected airfoils, *Bull. Acad. Pol. Sci.*, 25 (1977), 25–36 (591–602).
[43] R. Wegmann, On Fornberg's numerical method for conformal mapping, *SIAM J. Numer. Anal.*, **23** (1986), 1199–1213.
[44] ———, Methods for numerical conformal mapping, in *Handbook of Complex Analysis, Geometric Function Theory, Vol. 2*, (ed. R. Kuehnau), Elsevier, Amsterdam, (2005), 351–477.
[45] B. R. Williams, An exact test case for the plane potential flow about two adjacent lifting airfoils, *RAE Technical Report No. 3717*, London (1973).

Received xxxx 20xx; revised xxxx 20xx.

E-mail address: badreddine@math.wichita.edu
E-mail address: delillo@math.wichita.edu
E-mail address: sahraei@math.wichita.edu